THE ROYAL SOCIETY

Vapour nucleation in a cryogenic-fluid–dissolved-nitrogen mixture during rapid depressurization†

BY J. C. YANG[1], T. G. CLEARY[1], M. L. HUBER[2] AND W. L. GROSSHANDLER[1]

[1] *Building and Fire Research Laboratory, National Institute of Standards and Technology, Gaithersburg, MD 20899, USA*

[2] *Chemical Science and Technology Laboratory, National Institute of Standards and Technology, Boulder, CO 80303, USA*

Received 27 August 1997; accepted 28 September 1998

The behaviour of four cryogenic-fluid–dissolved-nitrogen mixtures inside a pressure vessel during rapid depressurization was investigated through experiment. The four fluids studied were CF_3I, FC-218 (C_3F_8), HFC-125 (C_2HF_5), and CF_3Br. Depressurization was achieved by discharging the liquid mixture through a solenoid valve at room temperature. Two initial total vessel pressures were used: (1) *ca.* 2.8 MPa and (2) *ca.* 4.2 MPa. Based on the experimental observations obtained by using a high-speed movie camera, the evolution of dissolved nitrogen was suggested for FC-218, HFC-125 and CF_3Br in the cases of initial total pressures of *ca.* 4.2 MPa. For initial vessel pressures of *ca.* 2.8 MPa, vapour nucleation was not observed for any of the four fluid–dissolved-nitrogen mixtures. No degassing was observed for CF_3I irrespective of the two initial total pressures. The predicted nucleation pressures based on the classical homogeneous nucleation theory for a binary-component mixture provided qualitative agreement with the observed vapour nucleation inside the vessel.

Keywords: cryogenic fluids; fire suppression; homogeneous nucleation; equation of state; fugacity

1. Introduction

Aircraft dry bays, which are cluttered with various electronic, mechanical and hydraulic components, are ventilated or unventilated compartments located along the wings and fuselage and adjacent to the fuel tank. Dry-bay fire threat is specific to military aircraft. The threat scenario arises during wartime missions, wherein an anti-aircraft incendiary round could pierce the dry-bay wall and could penetrate the fuel tank. Such a catastrophic event might lead to a deflagration and loss of the aircraft. Detection and suppression of dry-bay fires occur automatically (without pilot intervention) in less than 100 ms.

Current fire suppression bottles for dry-bay fire protection are normally filled with liquid halon 1301 (CF_3Br) to about half of the bottle volume, and the bottle is then pressurized with nitrogen to a specified total equilibrium pressure (typically

† Official contribution of the National Institute of Standards and Technology; not subject to copyright in the United States.

Table 1. *Thermophysical properties*

fluid	MW (g mol^{-1})	T_b (K)	T_c (K)	$10^6 P_c$ (Pa)	$10^6 P_{sat}$ (Pa)	ρ_c (g cm^{-3})	ρ_l (g cm^{-3})
CF_3I	196	251.2	395.2	4.04	0.49	0.871	2.106
FC-218	188	236.4	345.2	2.68	0.87	0.629	1.251
HFC-125	120	224.6	339.4	3.63	1.38	0.571	1.190
CF_3Br	149	215.4	340.2	4.02	1.61	0.745	1.551

4.2 MPa) at room temperature. The purposes of using the pressurization gas are to expedite the discharge of the agent, to facilitate the dispersion of the agent, and to maintain sufficient bottle pressure for low-temperature applications.

Due to nitrogen pressurization, nitrogen is dissolved in the liquid agent. The presence of dissolved nitrogen complicates the discharge process, in that the fluid leaving the vessel is not pure halon 1301, but a mixture of halon 1301 and nitrogen; in addition, the dissolved nitrogen comes out of the liquid in the form of bubbles inside the vessel during depressurization (discharge).

Halon 1301 is now banned from production in compliance with the *Montréal protocol on substances that deplete the ozone layer*. The search for halon alternatives has resulted in three potential agents for dry-bay fire-protection applications from a list of more than ten candidates (Grosshandler *et al.* 1994). These are the cryogenic fluids: HFC-125 (C_2HF_5), FC-218 (C_3F_8) and CF_3I. Table 1 (taken from Yang *et al.* (1995)), lists the thermophysical properties of these three fluids and CF_3Br.

During the course of the study on the rapid discharge and dispersion of these fire-suppressant–nitrogen mixtures from a pressurized container into a simulated dry bay, the behaviour of these mixtures inside the container during depressurization was also examined, because the conditions inside the vessel govern the subsequent expulsion process and external dispersion of the fire suppressant. In our previous study (Yang *et al.* 1996), the effect of dissolved nitrogen was not addressed. When no vapour nucleation or boiling inside the vessel occurred during depressurization, a simple two-stage (liquid followed by ullage vapour) discharge model was used to estimate the discharge rates, and the calculations were found to compare favourably with the experimental measurements. The present study is primarily concerned with the effect of a non-condensable gas (nitrogen) in a cryogenic fluid on the vapour nucleation inside a vessel during a rapid depressurization (of the order of 10 ms). This paper presents these experimental observations. Although the discharge of a pressurized liquid has been extensively studied in the context of loss-of-coolant accidents in nuclear reactors (e.g. Lienhard *et al.* 1978) and of hazard evaluations of sudden release of a cryogenic fluid stored under its own vapour pressure (e.g. Gühler *et al.* 1979), most of the studies use a single-component fluid (e.g. superheated water or pure refrigerants), and the time-scales vary from milliseconds to seconds.

2. Experimental methods

This section describes the experimental hardware and procedures used to perform the discharge tests. The depressurization experiments were performed at room temperature (22 °C ± 1 °C) in a room with dimensions of 3 m (width) × 3 m (length) ×

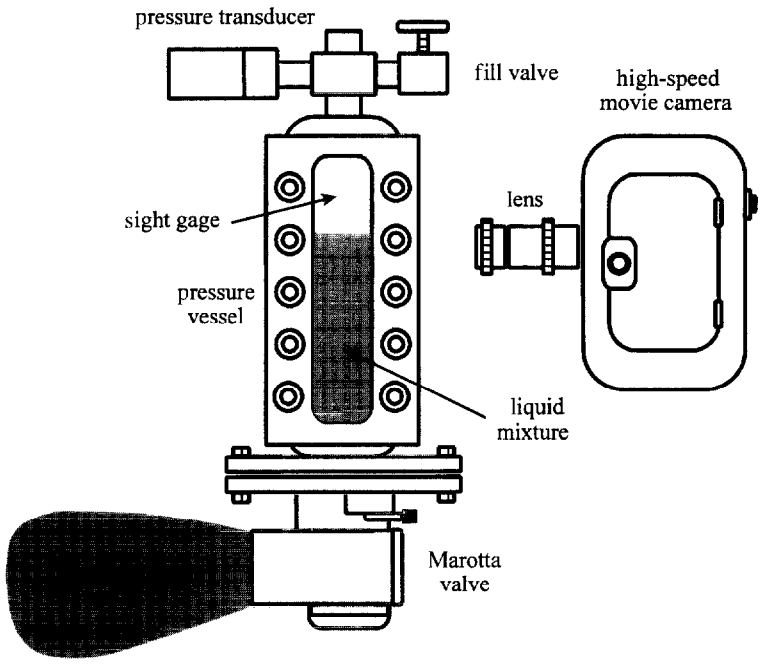

Figure 1. Experimental apparatus.

3.4 m (height). The pressure vessel was located on one side of the room, and its content was released directly into the room. Figure 1 is a schematic diagram of the experimental apparatus. The configuration used in the discharge experiments was bottom vented, i.e. the liquid portion in the vessel was released first.

The stainless-steel pressure vessel was equipped with two industrial liquid-level sight gauges for visual documentation of the behaviour of the dissolved-nitrogen–fluid mixture during depressurization. The internal volume of the vessel was measured to be 6.10×10^{-4} m^3 $\pm$ 5×10^{-6} m^3 (mean $\pm 2\sigma$).

A solenoid valve from Marotta Scientific (model MV121KJ-2)† was used to discharge the fire-suppressant–nitrogen mixtures from the pressure vessel. Fire-suppression systems in combat armoured vehicles are equipped with this type of solenoid valve. Upon activation, the valve with an outlet diameter of 4.45 cm remains open and requires re-arming if it is to be used again. Note that the valve has a smaller passage upstream of the outlet. Approximately 25 V and 10 A were required to activate the valve. The response time of the release mechanism was of the order of 10 ms.

The experimental preparation involved the following steps. The vessel was filled approximately two-thirds full (by volume). The total mass of the agent dispensed to the vessel, which was required to estimate the solubility of nitrogen in the cryogenic fluid, was obtained by weighing on an electronic scale with an uncertainty of 1 g. The vessel was then pressurized with nitrogen to a specified *equilibrium* pressure at room temperature. The attainment of the final equilibrium pressure could be facilitated

† Certain commercial products are identified in this paper in order to adequately specify the equipment used. Such identification does not imply recommendation by the National Institute of Standards and Technology, nor does it imply that this equipment is the best available for the purpose.

by shaking the vessel intermittently and vigorously and by repetitive nitrogen pressurization. The vessel was then mounted and was ready to be discharged at room temperature.

The temporal variation of the pressure inside the vessel during discharge was obtained using a piezoelectric dynamic-pressure transducer regulated by a dual-mode charge amplifier with a 180 kHz frequency filter or a fast-response static-pressure transducer. The outputs from the amplifiers and the static-pressure transducer (when used) were recorded using a 16-channel, 12-bit, high-speed data-acquisition board at a rate of 25 kHz per channel for 0.6 s. The data acquisition system was controlled by menu-driven software, and the data obtained were stored in a personal computer for subsequent analysis.

A high-speed movie camera equipped with a 45 mm lens and operating at 2000 frames per second was used to document the events occurring inside the vessel during depressurization. High-speed daylight films (ASA 400) together with two floodlights for front and back lighting were used.

The experimental sequence was controlled by a timing circuit. At the initiation of the timing sequence, the high-speed camera was first triggered to ensure that the full framing rate had been attained before photographing the depressurization process, and the camera was on for 2 s. At 0.8 s, the data acquisition was initiated for a duration of 0.6 s. At 1 s, the timing circuit sent a control signal to turn on the DC power supply for 0.2 s to activate the release mechanism.

The effect of the initial total charge pressure on the depressurization was examined by performing a series of experiments at room temperature with *ca.* 4.2 MPa (termed high-pressure discharge) and *ca.* 2.8 MPa (termed low-pressure discharge) total pressures.

3. Results and discussion

(*a*) *General visual observations*

The events occurring *inside* the vessel during a discharge of CF_3Br were *conceptually* described by Elliot *et al.* (1984) without any confirmation from visual observations. The initial vessel conditions ranged from 4.47 MPa at 12 °C to 10.24 MPa at 63 °C. Based on the experimental vessel pressure-decay curves during discharge and a simple theoretical flow model, several sequential events occurring inside the vessel were suggested. When the release mechanism was activated, there was a short period during which the pressure continuously decreased, and the liquid-CF_3Br–nitrogen mixture was expelled as a superheated liquid through the valve exit. Inside the vessel, nitrogen remained dissolved in the liquid agent as a non-equilibrium supersaturated solution, and the liquid–nitrogen mixture remained a clear solution. As the pressure inside the vessel dropped further, degassing of nitrogen in the solution occurred, and nitrogen bubbles started to form. Once the bubbles nucleated, the dissolved nitrogen quickly came out of the solution into the bubbles, causing the bubbles to grow. Due to rapid bubble expansion, the liquid level swelled, and the ullage was compressed to a higher pressure, which was noted as a short transient pressure recovery in the pressure-decay history. The pressure then began to decrease again until a transition point in the pressure-decay curve was reached. A bubbly two-phase CF_3Br–nitrogen mixture was assumed to be discharged from the vessel during this time-interval. The transition point signified the depletion of the two-phase mixture

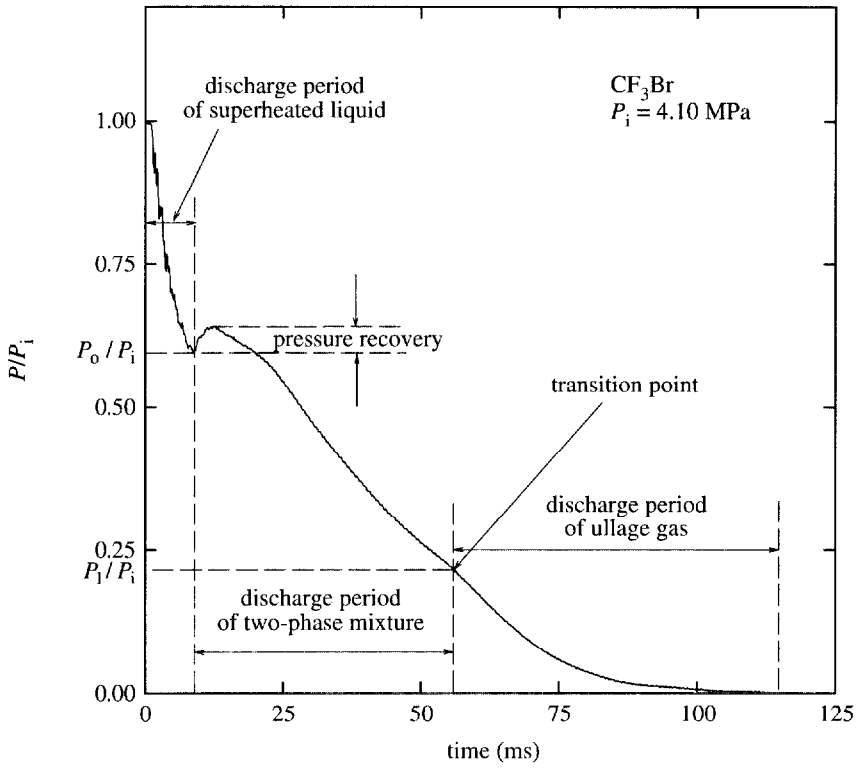

Figure 2. Illustration of a typical pressure-decay curve during depressurization (taken from Yang *et al.* 1995).

and the initiation of the discharge of the ullage gas mixture (CF_3Br vapour and nitrogen) from the vessel. Figure 2 is an illustration of a typical pressure-decay curve during a discharge. The extent of pressure recovery was found to be dependent upon the size of the opening of the discharge valve. For large valve openings, the pressure recovery was not noticeable, and a small plateau was observed in the pressure-decay curve (Yang *et al.* 1995).

The visual observations made in this study using high-speed photography revealed the following phenomena. For the higher pressure (*ca.* 4.2 MPa) discharges of CF_3Br, HFC-125 and FC-218, the liquid-agent–nitrogen mixture remained clear for a short duration (*ca.* 5 ms) after the initiation of the discharge. This duration was found to be dependent on the nature of the cryogenic fluid, with CF_3Br the shortest and FC-218 the longest. During this period, the receding liquid–vapour interface was clearly visible. The interior of the vessel as seen through the sight gauges then became completely foggy, and the liquid–vapour interface was no longer visible. It was not possible to determine from the movies that it was the frothing of the liquid mixture throughout the vessel due to vapour nucleation that initially caused the liquid–vapour interface to disappear; however, the time at which this event happened corresponded closely to that of the initiation of the pressure recovery in the pressure-decay curves. The fogginess was sustained for a period of time during which the liquid mixture was assumed to be completely discharged. The sight gauges on the vessel then became

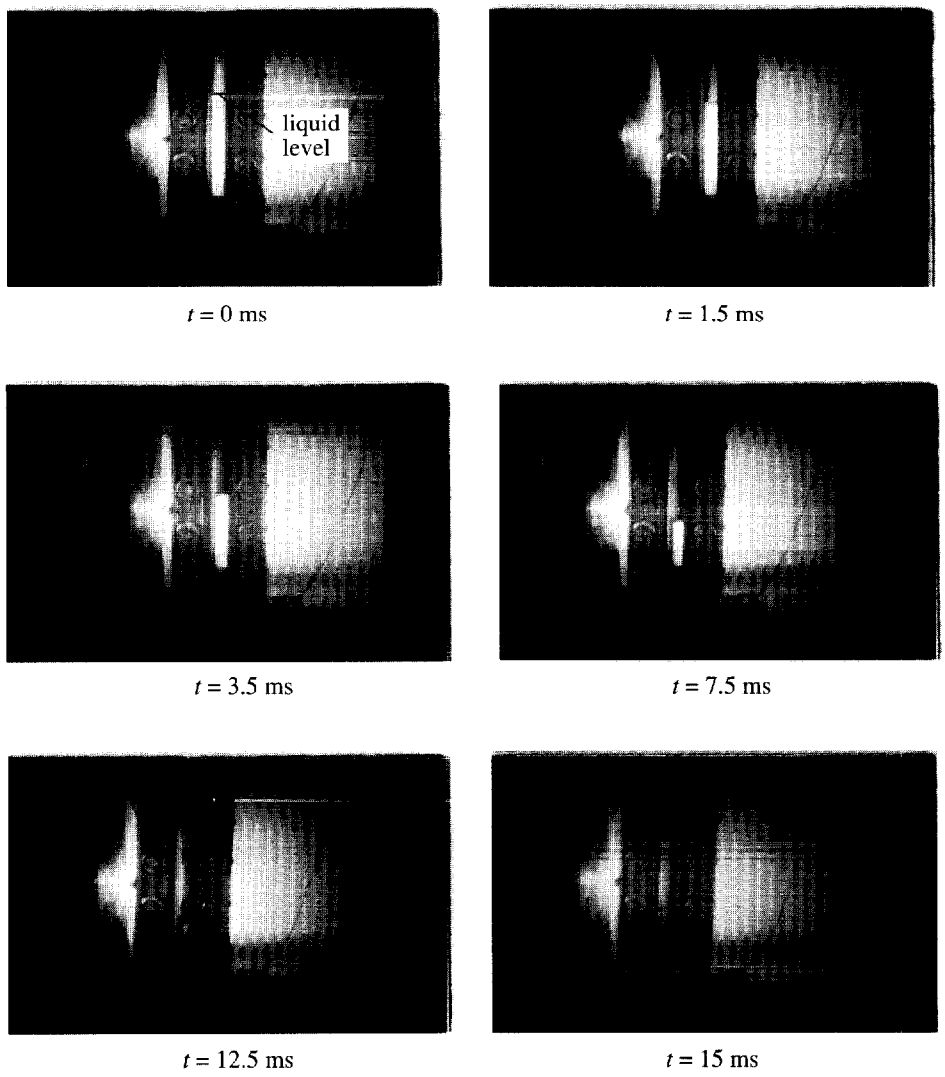

Figure 3. Photographic sequence of events observed through the sight gauge of the vessel during a high-pressure discharge of CF_3I.

clear once again. This fogginess is *conjectured* to be due both to vapour condensation as a result of cooling by the expansion of the ullage, and to the nucleation of vapour in the bulk liquid. The existence of the vapour bubbles could not be visually confirmed from the high-speed movies due to the limited spatial resolution of the pictures. For CF_3I, the receding liquid–vapour interface and the liquid mixture remained clear for a relatively long time after the initiation of the discharge. The fogginess then appeared throughout the vessel, and the liquid–vapour interface was no longer visible. The interior of the vessel became clear again after a period of fogginess. It was postulated that vapour nucleation did not occur in the CF_3I–nitrogen mixture (see discussion below). No pressure recovery was noted in the pressure-decay curves for

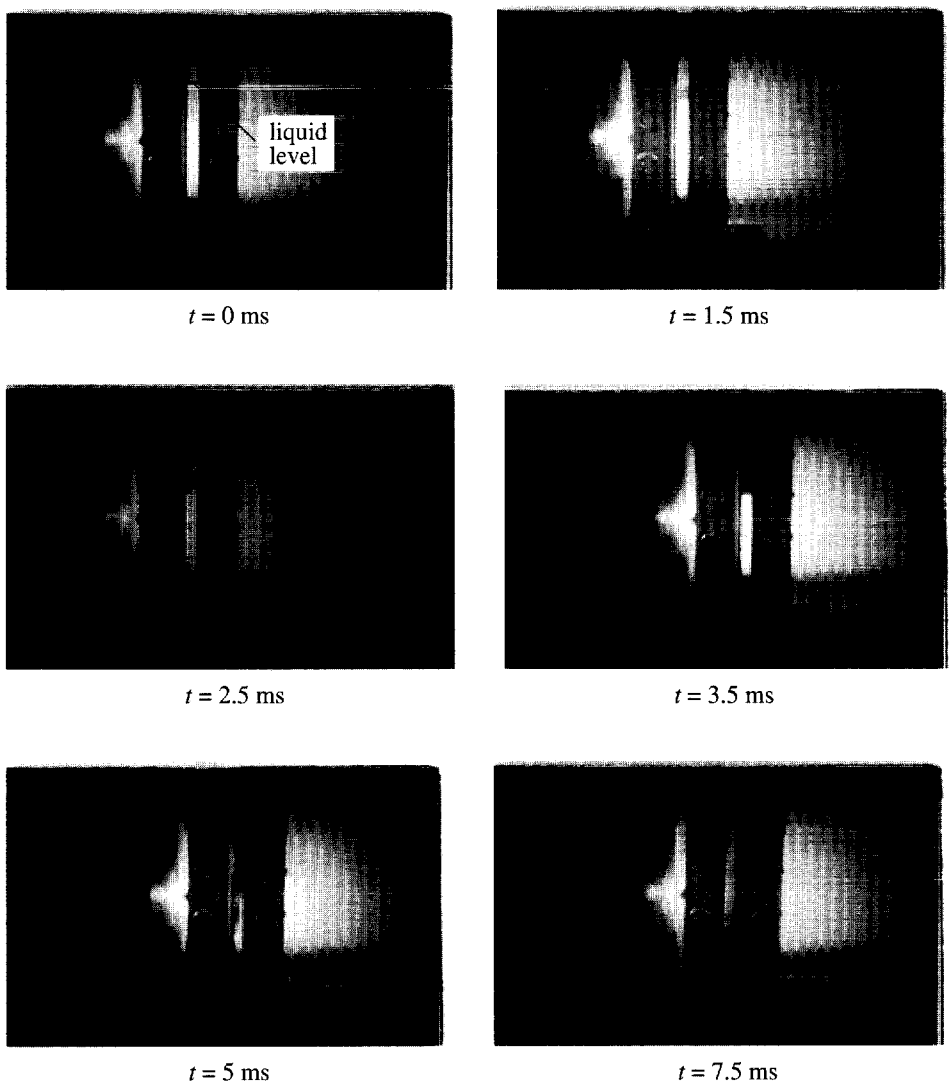

Figure 4. Photographic sequence of events observed through the sight gauge of the vessel during a high-pressure discharge of FC-218.

the CF_3I–nitrogen mixture. Figures 3–6 are selected photographic sequences of events for CF_3I–N_2, FC-218–N_2, HFC-125–N_2 and CF_3Br–N_2 mixtures, respectively.

For the lower-pressure (*ca.* 2.8 MPa) discharges, no pressure recovery was recorded in the pressure-decay curves for any of the fluid–dissolved-nitrogen mixtures studied (Yang *et al.* 1995), and the high-speed movies revealed similar phenomena to those observed in the high-pressure (*ca.* 4.2 MPa) discharges for the same fluid–nitrogen mixture, except that the liquid–vapour interface remained visible and clear for a much longer duration, implying that no degassing occurred during depressurization. Representative photographic sequences of events are shown in figures 7–10 for the four fluid–nitrogen mixtures, respectively.

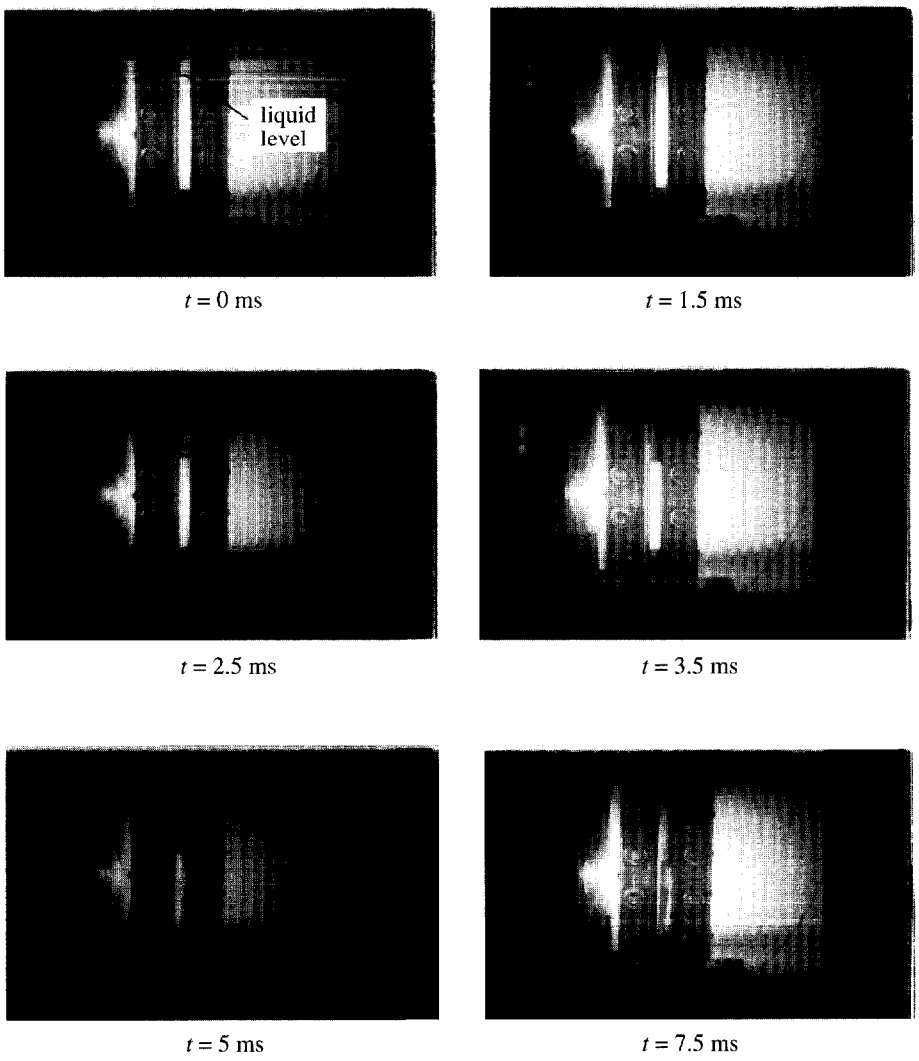

Figure 5. Photographic sequence of events observed through the sight gauge of the vessel during a high-pressure discharge of HFC-125.

(*b*) *Bubble nucleation*

Classical homogeneous nucleation theory is used in an attempt to assess the role of non-condensable gas on the vapour nucleation inside the vessel during depressurization. The application of the homogeneous nucleation theory is based on the assumptions that the fluids contain no impurities, that these low-surface-tension ($\sigma < 10$ dyn cm^{-1} at 22 °C) cryogenic fluids wet the surface of the vessel wall with ease, and that the initial rate of depressurization is relatively rapid (*ca.* 400 MPa s^{-1}). The absence of impurities implies the lack of heterogeneous nucleation sites in the bulk liquid. The low surface tension of the fluid may also reduce heterogeneous nucleation sites at the liquid–vessel-wall interface, because the irregular cavities on

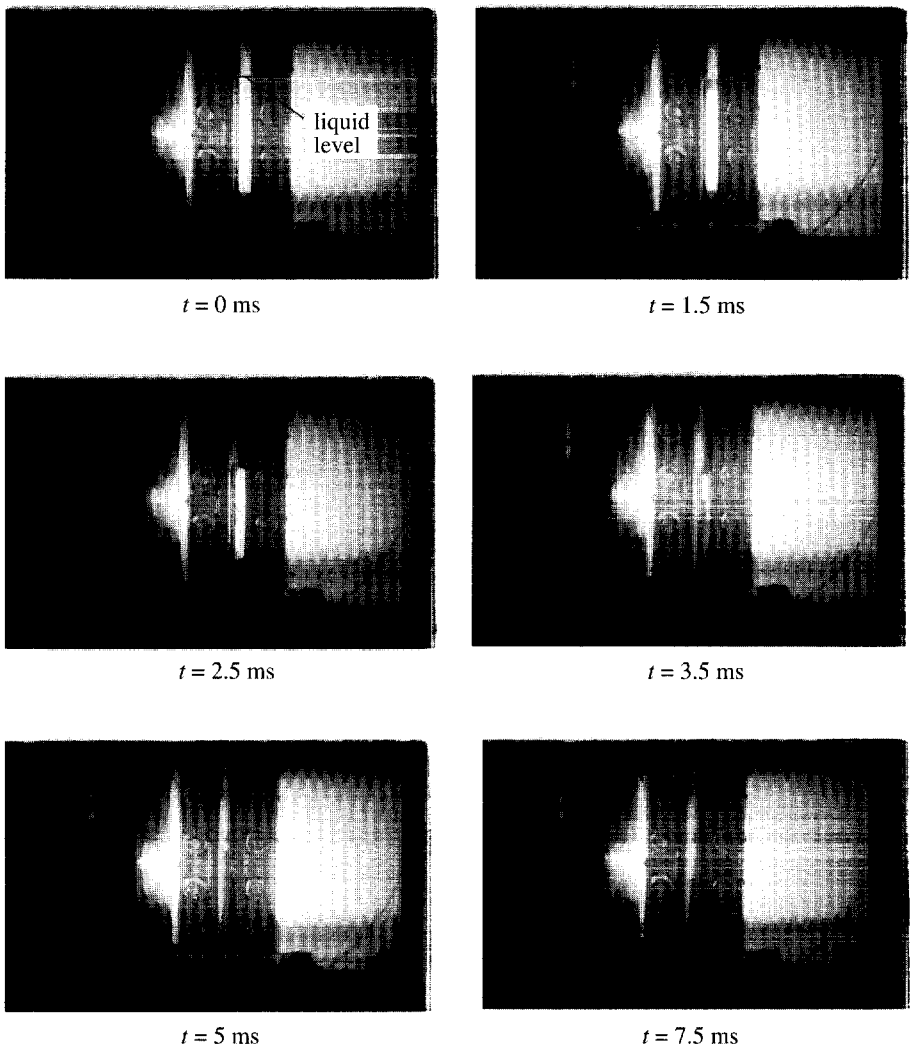

Figure 6. Photographic sequence of events observed through the sight gauge of the vessel during a high-pressure discharge of CF_3Br.

the imperfect vessel surface will be expected to trap vapour less effectively (Carey 1992). The rapid depressurization rate may cause the heterogeneous sites to remain relatively inactive (Elias & Chambré 1993). Even if heterogeneous nucleation is probable, the classical homogeneous nucleation theory may, in principle, still be applied by incorporating an empirical heterogeneity correction factor (Blander & Katz 1975). It should be emphasized that the intent here is not to delineate the roles of homogeneous and heterogeneous nucleation, but rather to offer a plausible qualitative explanation for the observed phenomena.

The problem to be considered may now be formulated as follows. A vessel initially containing a two-phase binary component (cryogenic-fluid–dissolved-nitrogen) mixture is undergoing rapid depressurization. The initial temperature (T_i), total pressure

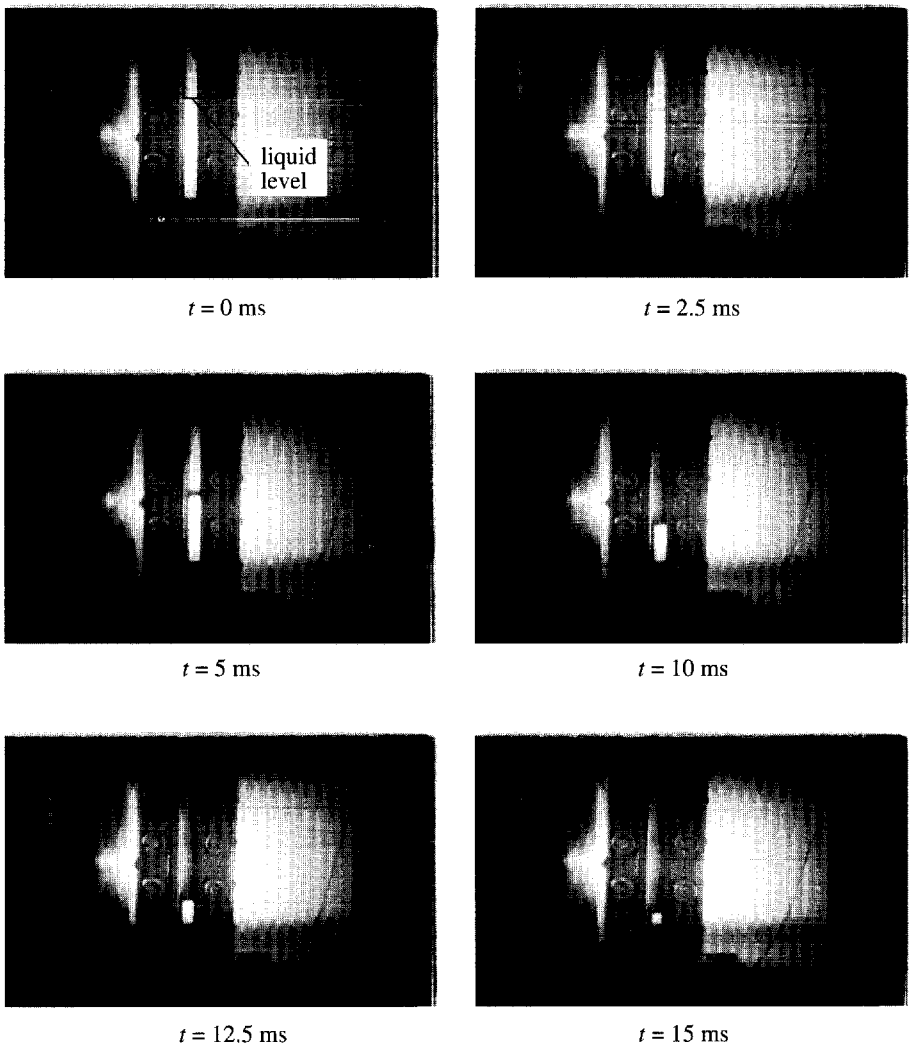

Figure 7. Photographic sequence of events observed through the sight gauge of the vessel during a low-pressure discharge of CF_3I.

(P_i) and mole fraction of dissolved nitrogen (X_n) are known. Since depressurization is very rapid, the process occurring in the liquid phase can be considered to be isothermal. Figure 11 illustrates the initial vessel conditions and a gas bubble (size being exaggerated) in equilibrium with the superheated liquid. The system to be considered is depicted in the enlarged view in figure 11. Two major assumptions have been applied in the figure: (1) the amount of liquid in the container is considered to be a closed system at any instant in time; and (2) the number of molecules in the vapour nucleus is negligibly small, such that the liquid compositions remain unchanged at bubble nucleation (Ward *et al.* 1970; DeBenedetti 1996).

The critical-size nucleus, once formed, is defined to be in unstable thermodynamic equilibrium with the surrounding superheated liquid; therefore, the fugacities of each

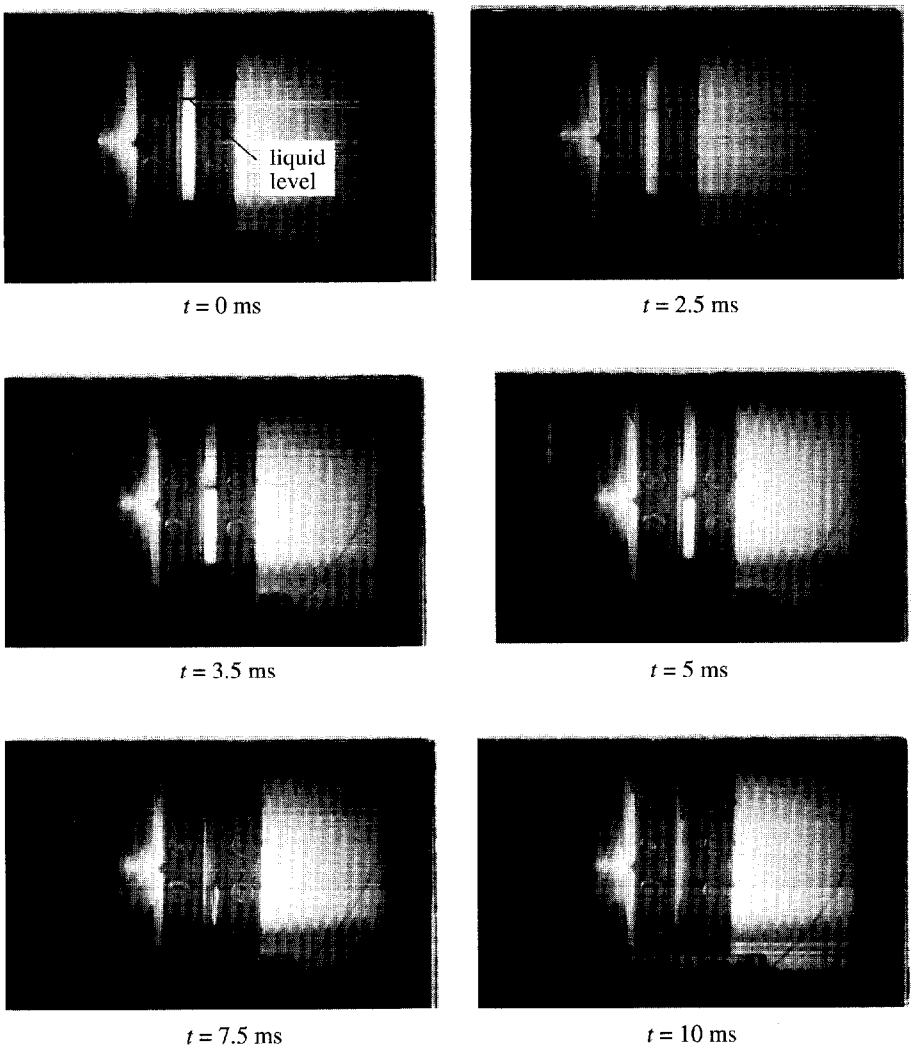

Figure 8. Photographic sequence of events observed through the sight gauge of the vessel during a low-pressure discharge of FC-218.

component are equal in the liquid and vapour phases (Modell & Reid 1983):

$$f_{\mathrm{n}}^{\mathrm{L}}(P_0, T_{\mathrm{i}}, X_{\mathrm{n}}) = f_{\mathrm{n}}^{\mathrm{V}}(P_{\mathrm{b}}, T_{\mathrm{i}}, Y_{\mathrm{n}}); \tag{3.1}$$

$$f_{\mathrm{a}}^{\mathrm{L}}(P_0, T_{\mathrm{i}}, X_{\mathrm{a}}) = f_{\mathrm{a}}^{\mathrm{V}}(P_{\mathrm{b}}, T_{\mathrm{i}}, Y_{\mathrm{a}}). \tag{3.2}$$

In addition, the pressure differential across the bubble interface is given by the Young–Laplace equation:

$$P_{\mathrm{b}} - P_0 = 2\sigma/R_{\mathrm{c}}. \tag{3.3}$$

Since there are four unknowns $(P_{\mathrm{b}}, P_0, Y_{\mathrm{n}}, R_{\mathrm{c}})$ in the above three equations, one more equation is needed. This equation is obtained from the consideration of the kinetics of the superheat limit of a binary mixture (Holden & Katz 1978). The

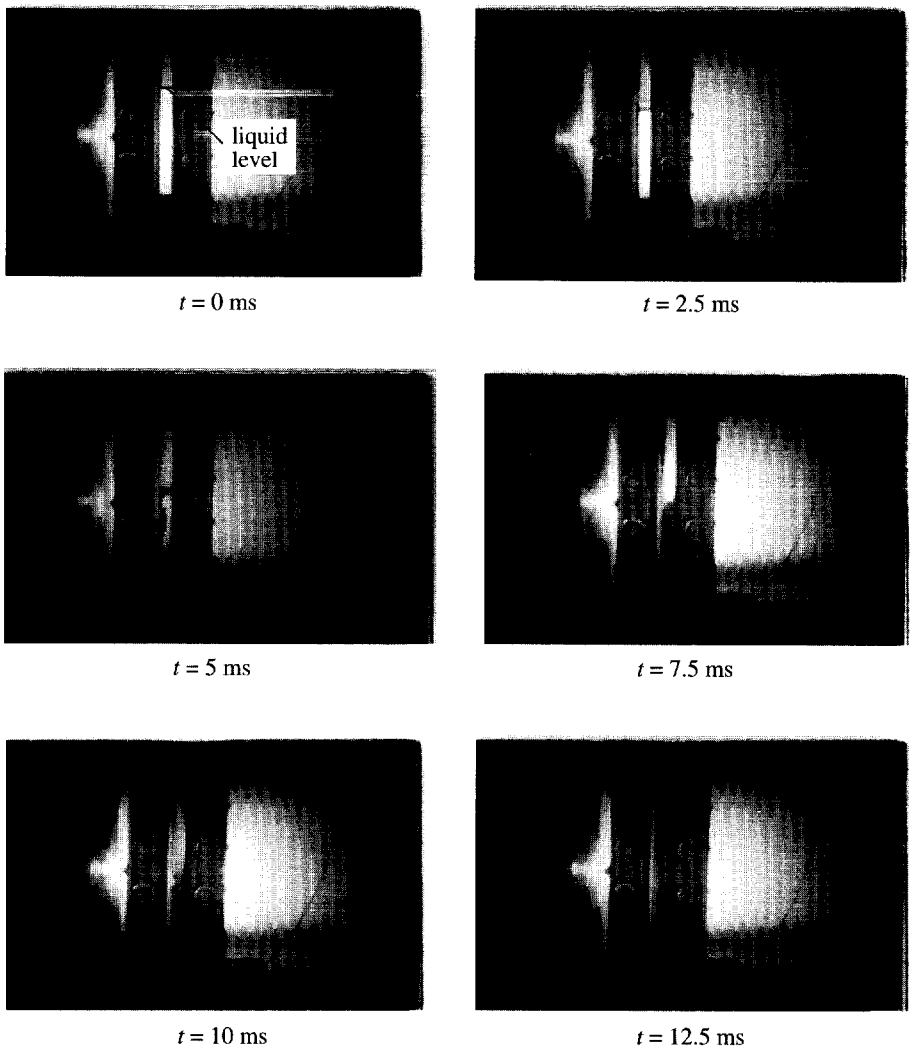

Figure 9. Photographic sequence of events observed through the sight gauge of the vessel during a low-pressure discharge of HFC-125.

nucleation rate, J, is given by

$$J = \frac{N_A}{v^L}\left(\frac{Y_a}{\sqrt{m_a}} + \frac{Y_n}{\sqrt{m_n}}\right)\left(\frac{2\sigma}{\pi}\right)^{1/2} \exp\left[\frac{-4\pi\sigma R_c^2}{3kT_i}\right]. \tag{3.4}$$

To solve for the pressures inside and outside the bubble, the mole fractions inside the vapour nucleus, and the critical radius, a condition wherein R_c is assumed to be infinite is first examined (see figure 12). Again, from phase equilibria (Prausnitz *et al.* 1986)

$$[f_a^L(P_e, T_i, X_a)]_{R_c\to\infty} = [f_a^V(P_e, T_i, Y_{ea})]_{R_c\to\infty}, \tag{3.5}$$

$$[f_n^L(P_e, T_i, X_n)]_{R_c\to\infty} = [f_n^V(P_e, T_i, Y_{en})]_{R_c\to\infty}. \tag{3.6}$$

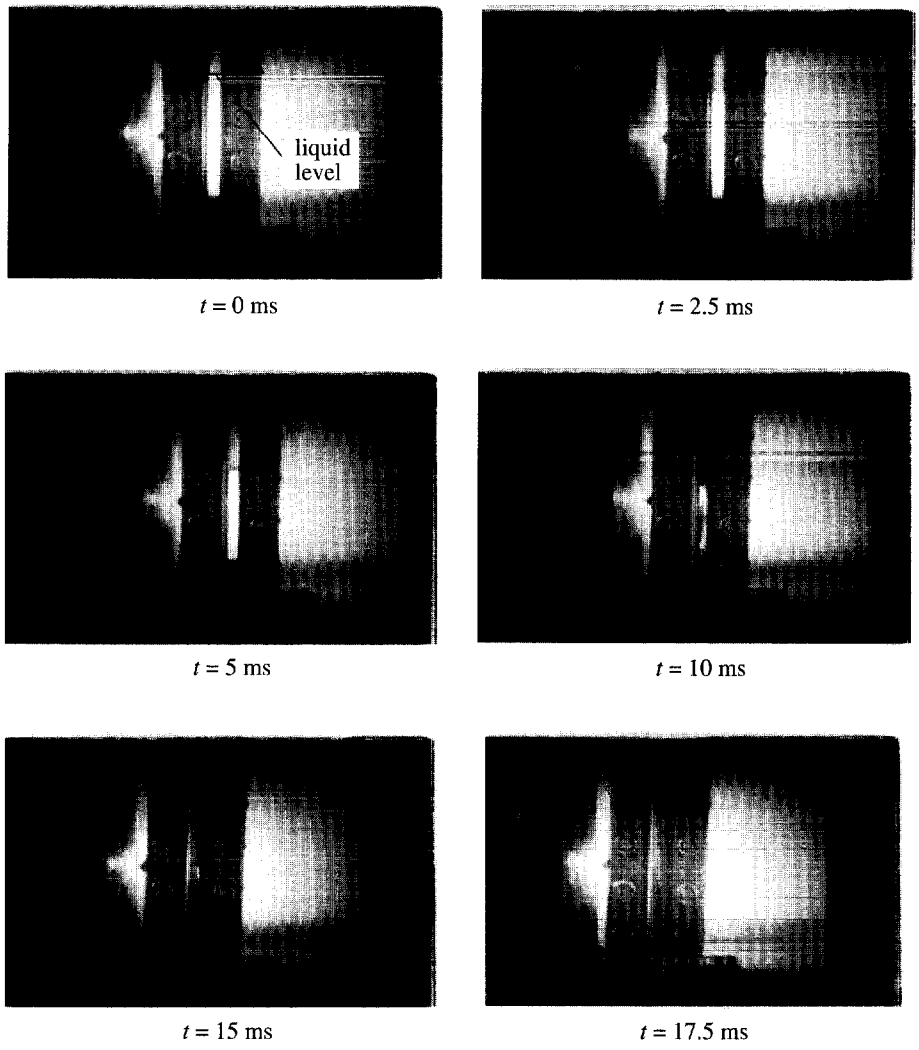

Figure 10. Photographic sequence of events observed through the sight gauge of the vessel during a low-pressure discharge of CF_3Br.

In the above equations, the independent variables are explicitly stated for clarification; however, in what follows, the functional arguments will be omitted for simplicity. From thermodynamics (Modell & Reid 1974),

$$\left[\frac{\partial \ln f_i}{\partial P}\right]_{T_i} = \frac{\bar{v}_i}{RT_i}. \tag{3.7}$$

Therefore,

$$RT_i \int_{[f_a^L]_{R_c}}^{f_a^L} d\ln f_a^L = \int_{P_c}^{P_0} \bar{v}_a^L \, dP. \tag{3.8}$$

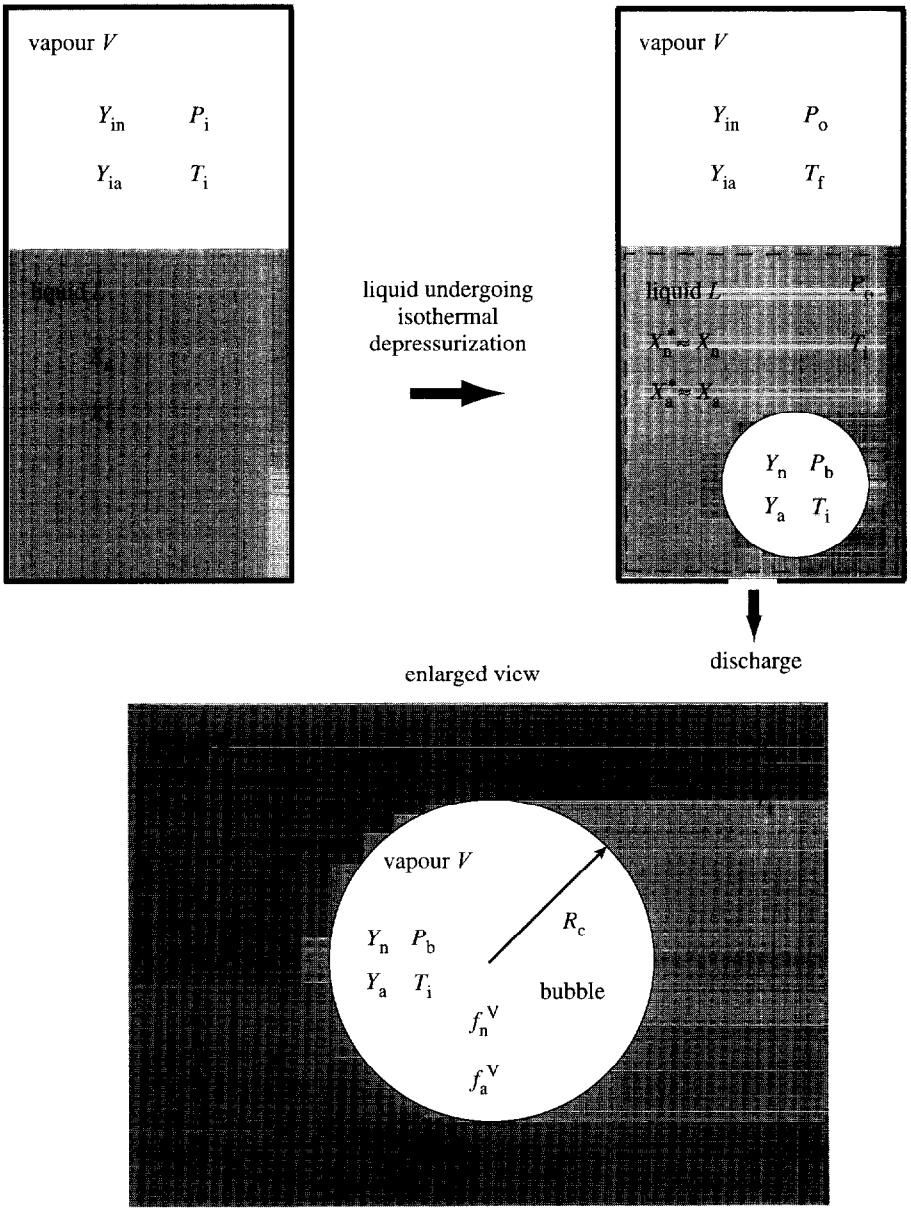

Figure 11. Schematic diagram of the system considered in the analysis of the formation of a vapour embryo by homogeneous nucleation.

If the partial molar volume of the agent, $\bar{v}_a^L$, is assumed to be only a function of temperature (i.e. a weak function of pressure and composition), then equation (3.8) becomes

$$f_a^L = [f_a^L]_{R_c \to \infty} \exp\left[\frac{\bar{v}_a^L (P_0 - P_e)}{RT_i}\right]. \tag{3.9}$$

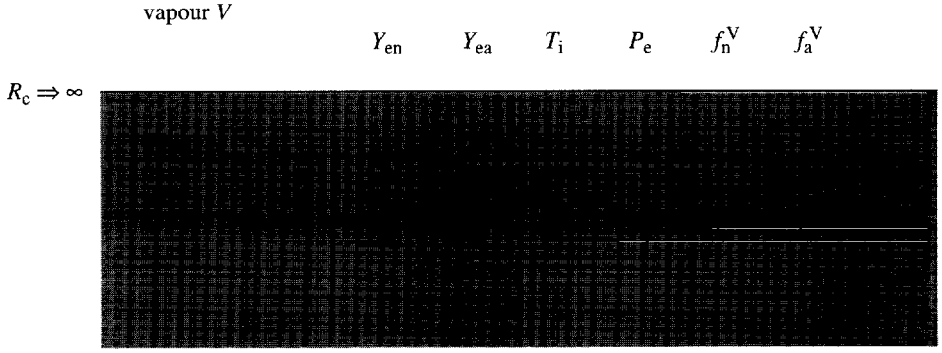

Figure 12. Thermodynamic equilibrium across a flat surface for given T_i, X_n and X_a.

Substituting equations (3.2) and (3.5) into equation (3.9), we obtain

$$f_a^V = [f_a^V]_{R_c \to \infty} \exp\left[\frac{\bar{v}_a^L(P_0 - P_e)}{RT_i}\right]. \tag{3.10}$$

Further simplification of equation (3.10) results if, according to Modell & Reid (1974),

$$\frac{f_a^V}{[f_a^V]_{R_c \to \infty}} \approx \frac{Y_a P_b}{Y_{ea} P_e}. \tag{3.11}$$

The terms $Y_a P_b$ and $Y_{ea} P_e$ are simply the partial pressures. Equation (3.10) becomes

$$Y_a P_b = Y_{ea} P_e \exp\left[\frac{\bar{v}_a^L(P_0 - P_e)}{RT_i}\right]. \tag{3.12}$$

Similarly, an expression for the partial pressure of nitrogen in the vapour nucleus can be derived:

$$Y_n P_b = Y_{en} P_e \exp\left[\frac{\bar{v}_a^L(P_0 - P_e)}{RT_i}\right]. \tag{3.13}$$

In the case of $R_c \to \infty$, with X_a and T_i given, P_e and Y_{ea} can be determined from vapour–liquid equilibrium calculations with a known equation of state, or by the methods described in Prausnitz *et al.* (1980). The partial pressures (or mole fractions) in the vapour nucleus can then be calculated using equations (3.12) and (3.13). Once P_e and Y_{ea} are known, P_0 can be determined using equations (3.3), (3.4), (3.12) and (3.13) with a given J.

Since the Peng–Robinson equation of state (EOS) has been used to calculate and correlate vapour–liquid equilibrium data for refrigerant–dissolved-nitrogen mixtures (Abu-Eishah 1991), it was used here to estimate the homogeneous nucleation pressure. A detailed calculation procedure is given in Appendix A.

The experimental homogeneous nucleation pressure data from Forest & Ward (1977, 1978) were used to check the validity of the current computational scheme. The measurements from Forest & Ward (1977, 1978) were obtained by subjecting a suspended-liquid-ethyl-ether–dissolved-nitrogen droplet to isothermal depressurization in a glycerine host liquid. As shown in table 2, the calculated homogeneous nucleation pressures for ethyl-ether–nitrogen using the current method are found to be comparable (with an overall deviation of 4%) to the measured values obtained by Forest & Ward (1977, 1978), even without taking the proper values of the binary

Table 2. *Comparison between measured and calculated P_0 ($J = 10$ nuclei cm^{-3} s^{-1}) for ethyl-ether–nitrogen mixture*

X_n	T_i (K)	measured $10^6 P_0$ (Pa) (Forest & Ward 1977, 1978)	calculated $10^6 P_0$ (Pa) (present method)
0	419.2	0.211	0.271
0.0042	419.2	0.402	0.417
0.0109	419.2	0.695	0.648
0.0187	419.2	1.102	0.915
0	426.2	0.777	0.841
0.0057	426.2	0.978	1.029
0.0137	426.2	1.273	1.294
0.0244	426.2	1.710	1.645
0	433.5	1.366	1.408
0.0067	433.5	1.557	1.618
0.0168	433.5	1.851	1.936
0.0299	433.5	2.290	2.342
0	443.2	2.089	2.122
0.0091	443.2	2.239	2.385
0.0237	443.2	2.564	2.800
0.0413	443.2	3.012	3.296

Table 3. *Observed and calculated P_0 at $T_i = 294$ K for the four cryogenic fluids*

fluid	$10^6 P_i$ (Pa)	X_n	$10^6 P_l$ (Pa) (observed)[a]	$10^6 P_0$ (Pa) (observed)[a]	$10^6 P_0$ (Pa) (predicted)
CF_3I	4.24	0.089	0.97	none	−3.97
FC-218	4.20	0.154	—[b]	2.50	1.56
HFC-125	4.21	0.106	—[b]	2.38	1.36
CF_3Br	4.18	0.093	—[b]	2.33	1.68
CF_3I	2.86	0.057	0.73	none	−5.02
FC-218	2.93	0.097	1.11	none	0.52
HFC-125	2.93	0.060	0.94	none	0.46
CF_3Br	2.84	0.047	0.86	none	0.53

[a]From Yang *et al.* (1995).
[b]Unable to identify the transition point from the pressure trace with certainty, but P_l (observed) is still less than P_0 (predicted).

interaction coefficients (i.e. $\delta_{ij} = 0$). To carry out the calculations, the mole ratios, C, used in Forest & Ward (1977, 1978) were converted to X_n by the following equation:

$$X_n = C/(1 + C). \tag{3.14}$$

Table 3 shows the calculated results based on the experimental conditions used to obtain figures 3–10. The calculated homogeneous nucleation pressures for CF_3I nitrogen mixtures were found to be negative (i.e. in tension); negative homogeneous nucleation pressures are possible (Reid 1976), although at present no experimental data on CF_3I–nitrogen mixtures are available to substantiate the predictions. Negative homogeneous nucleation pressures were also obtained when the treatment

developed by Forest & Ward (1977) was used (Yang *et al.* 1995). The observed P_0 were obtained from the experimental pressure-decay curves (see figure 2 and Yang *et al.* (1995)). The pressures at the transition point (P_1) of the pressure-decay curves are also tabulated in table 3. The uncertainties associated with the pressure readings were estimated to be less than 0.1 MPa. However, the transition points were not distinct in some cases, making it very difficult to extract the P_1 readings with certainty from the pressure-decay curves.

In order to interpret, qualitatively, the experimental observations in terms of the aforementioned homogeneous nucleation theory, we make use of the following assumptions, which are based partly on the experimental observations:

1. P_0 (measured) signifies the initiation of vapour nucleation inside the vessel;
2. if P_1 (measured) $> P_0$ (calculated), bubble nucleation is not possible because there will be no liquid mixture remaining in the vessel when the pressure reaches P_0; and
3. the absence of measured P_0 and the observation of a clear meniscus in the sight gauge for a long period of time implies the non-occurrence of vapour nucleation inside the vessel during depressurization.

Based on the calculated homogeneous nucleation pressures in table 3, vapour nucleation in CF_3I–nitrogen liquid mixtures was predicted not to occur during either high- or low-pressure discharges, and it was not observed experimentally under the same experimental conditions (as shown in figures 3 and 7).

At the low initial charge pressure ($P_i \sim 2.8$ MPa), there was no indication of degassing from the pressure-decay curves using any of the four fluids. The homogeneous nucleation theory, discussed above, also predicted no degassing ($P_1 > P_0$). For high initial charge pressure ($P_i \sim 4.2$ MPa), the experimental pressure-decay curves indicated vapour nucleation inside the vessel when FC-218, HFC-125 and CF_3Br were used, which was in accordance with the prediction from homogeneous nucleation theory ($P_1 < P_0$).

4. Conclusions

Based on the experimental observations and the interpretation of the experimental data by the homogeneous nucleation theory, the following conclusions can be made.

1. For FC-218, HFC-125 and CF_3Br–nitrogen mixtures at an initial total vessel pressure of *ca.* 4.2 MPa, a clear liquid mixture and a meniscus were no longer observable a short time ($O(1)$ ms) after depressurization commenced, an indication of bubble nucleation. However, this phenomenon was not observed when a CF_3I–nitrogen mixture was used.
2. At an initial total vessel pressure of *ca.* 2.8 MPa, a clear liquid mixture and a meniscus were observed for a long period of time for the four liquid mixtures, an indication of no degassing during depressurization.
3. Although the calculated nucleation pressures from homogeneous nucleation theory were lower than the measured values, the predicted trends appeared to follow the experimental observations.

The ability to predict the non-occurrence of vapour nucleation under certain initial vessel conditions using homogeneous nucleation theory can, therefore, facilitate the calculations of the discharge rates of the fluid–dissolved-nitrogen mixtures by using a simple two-stage discharge model.

This work was funded by the United States Air Force, Army and Navy and the Federal Aviation Administration. Their financial support was greatly appreciated. The authors thank Roy McLane and William Rinkinen (retired) of NIST for fabricating some of the experimental hardware and for assisting in performing some of the experiments, and Professor C. A. Ward of the University of Toronto for many helpful discussions.

Appendix A.

The Peng–Robinson equation (Peng & Robinson 1976) in its original form is given by

$$P = \frac{RT}{v-b} - \frac{a}{v(v+b)+b(v-b)}. \tag{A 1}$$

Equation (A 1) can be rewritten in terms of the compressibility factor Z, as follows:

$$Z^3 - (1-B)Z^2 + (A - 3B^2 - 2B)Z - (AB - B^2 - B^3) = 0, \tag{A 2}$$

where a, b, A and B are the parameters the expressions of which can be found in the original paper by Peng & Robinson (1976). In the two-phase region, equation (A 2) yields three real roots with the largest root being the vapour-phase Z and the smallest root being the liquid-phase Z.

For a binary-component mixture with mole fractions X_1 and X_2, the parameters a and b can be defined by using the following mixing rules

$$a = \sum_{i=1}^{2}\sum_{j=1}^{2} X_i X_j a_{ij}, \tag{A 3}$$

$$b = \sum_{i=1}^{2} X_i b_i, \tag{A 4}$$

where

$$a_{ij} = (1-\delta_{ij}) a_i^{1/2} a_j^{1/2}. \tag{A 5}$$

Note that $a_{ij} = a_{ji}$, $a_{ii} \equiv a_i$, and a_i and b_i are the parameters a and b for the pure component i, respectively. In equation (A 5), δ_{ij} is an empirically determined binary interaction coefficient. The fugacity of component i in a binary mixture with mole fractions X_1 and X_2 at P, T can be calculated from the following equation:

$$\ln\frac{f_i}{X_i P} = \frac{b_i}{b}(Z-1) - \ln(Z-B) - \frac{A}{2\sqrt{2}B}\left[\left(2\sum_{j=1}^{2} X_j a_{ji} \Big/ a\right) - \frac{b_i}{b}\right] \ln\left[\frac{Z+2.414B}{Z-0.414B}\right]. \tag{A 6}$$

Given T_i and X_a, and using equations (3.5), (3.6) and (A 6), Y_ea, Y_en and P_e can be determined. The calculation procedure, which is the determination of bubble-point

pressure, can be found in Walas (1985). The partial molar volumes can be calculated by using the following two equations (Walas 1985):

$$\bar{v}_{\mathrm{a}}^{\mathrm{L}} = \frac{RT}{P}\left[Z + X_{\mathrm{n}}\left(\frac{\partial Z}{\partial X_{\mathrm{a}}}\right)_{T,P}\right], \tag{A 7}$$

$$\bar{v}_{\mathrm{n}}^{\mathrm{L}} = \frac{RT}{P}\left[Z - X_{\mathrm{a}}\left(\frac{\partial Z}{\partial X_{\mathrm{a}}}\right)_{T,P}\right]. \tag{A 8}$$

The derivative of Z with respect to mole fraction can be obtained from equation (A 2). In the calculations, the liquid molar and partial molar volumes are assumed to be independent of pressure, and the binary interaction coefficient δ_{ij} is set equal to zero due to the lack of vapour–liquid equilibrium experimental data for these cryogenic-fluid–dissolved-nitrogen mixtures in the literature.

For given T_{i}, X_{a}, J and X_{n}, the following computational procedure for calculating the homogeneous nucleation pressure may be followed.

Step 1. Calculate P_{e}, Y_{ea} and Y_{en} (bubble-point-pressure calculation) using equations (3.5), (3.6) and (A 6).

Step 2. Calculate $Z(P_{\mathrm{e}}, T_{\mathrm{i}}, X_{\mathrm{a}})$ using equation (A 2).

Step 3. Calculate $\bar{v}_{\mathrm{a}}^{\mathrm{L}}(P_{\mathrm{e}}, T_{\mathrm{i}}, X_{\mathrm{a}})$ and $\bar{v}_{\mathrm{n}}^{\mathrm{L}}(P_{\mathrm{e}}, T_{\mathrm{i}}, X_{\mathrm{n}})$ using equations (A 7) and (A 8).

Step 4. Calculate $v^{\mathrm{L}}(P_{\mathrm{e}}, T_{\mathrm{i}}, X_{\mathrm{a}})$ using $Z(P_{\mathrm{e}}, T_{\mathrm{i}}, X_{\mathrm{a}})$, P_{e} and T_{i}.

Step 5. Assume P_0 (= 0.1 MPa).

Step 6. Calculate P_{b}, Y_{a} and Y_{n} using equations (3.12) and (3.13).

Step 7. Calculate new P_0 using equations (3.3) and (3.4).

Step 8. Is $|P_0^{\mathrm{new}} - P_0^{\mathrm{old}}| < 0.001$? If yes, stop; if no, $P_0 = P_0^{\mathrm{new}}$, and go to step 6.

The surface tension for pure agent estimated by the method of Brock & Bird (Reid *et al.* 1987) was used in the calculation of P_0; the effect of the dissolved nitrogen on the surface tension is assumed to be negligible. A value of J has to be assigned in order to carry out the calculations. Fortunately, J is inside the logarithmic term when P_0 is solved from equation (3.4), and the calculated homogeneous nucleation pressure is not very sensitive to the exact value of J. The nucleation rate J commensurate with our experimental conditions can be estimated in terms of a waiting time τ, which is defined as the time one must wait for a critical-size nucleus to form in the metastable superheated liquid at a given temperature and pressure (Skripov 1974). Then, $\tau \sim 1/(JV)$, where V is the volume of the superheated liquid. If we assume that, in our experiments, the evolution of dissolved nitrogen in the liquid mixture starts at the initiation of the pressure recovery in the pressure-decay curve (see figure 2), then the time to reach P_0 in figure 2 can be considered as the waiting time. With $V \sim O(100)$ cm^3 and $\tau \sim O(10)$ ms as observed in our experiments, the nucleation rate J is estimated to be $O(1)$ nuclei cm^{-3} s^{-1}. Therefore, $J \approx 1$ nuclei cm^{-3} s^{-1} was used in the calculations of homogeneous nucleation pressures.

In our experimental procedure, the only known parameters are T_{i} and P_{i}, the volume of the vessel, and the initial amount of pure cryogenic fluid (before nitrogen pressurization). Since we did not measure the concentration of dissolved nitrogen

in the liquid mixture after nitrogen pressurization, X_n was calculated by using an existing predictive model that is based on an extended corresponding-states principle (Yang *et al.* 1997).

Nomenclature

C	mole ratio of dissolved nitrogen to fluid, dimensionless
f	fugacity (Pa)
J	nucleation rate (nuclei $\mathrm{cm^{-3}\ s^{-1}}$)
k	Boltzmann's constant ($1.380\,48 \times 10^{-23}\ \mathrm{J\ K^{-1}}$)
m	molecular mass (g)
MW	molecular weight ($\mathrm{g\ mol^{-1}}$)
N_A	Avogadro's number (6.023×10^{23} molecule $\mathrm{mol^{-1}}$)
P_b	pressure inside the vapour nucleus (Pa)
P_c	critical pressure (Pa)
P_e	bubble-point pressure (Pa)
P_i	initial pressure of vessel (Pa)
P_0	homogeneous nucleation pressure (Pa)
P_{sat}	vapour pressure of pure cryogenic fluid at 25 °C (Pa)
R	universal gas constant ($8\,314\,390\ \mathrm{Pa\ cm^3\ mol^{-1}\ K^{-1}}$)
R_c	critical radius of the vapour nucleus (cm)
T	temperature (K)
T_b	normal boiling point (K)
T_c	critical temperature (K)
T_f	ullage temperature at vapour nucleation (K)
T_i	initial temperature of vessel (K)
v	molar volume ($\mathrm{cm^3\ mol^{-1}}$)
v^L	liquid molar volume ($\mathrm{cm^3\ mol^{-1}}$)
$\bar{v}^L$	liquid partial molar volume ($\mathrm{cm^3\ mol^{-1}}$)
V	volume of the superheated liquid ($\mathrm{cm^3}$)
X	liquid phase mole fraction or mole fraction in general (dimensionless)
Y	vapour phase mole fraction (dimensionless)
Z	compressibility factor (dimensionless)

Greek letters

δ_{ij}	binary interaction coefficient (dimensionless)
ρ_c	critical density ($\mathrm{g\ cm^{-3}}$)
ρ_l	saturated liquid density at 25 °C ($\mathrm{g\ cm^{-3}}$)
σ	surface tension ($\mathrm{dyn\ cm^{-1}}$)
τ	waiting time (ms)

Subscripts

a	cryogenic fluid
e	saturation conditions
i	component i
i	initial condition

j	component j
n	nitrogen

Superscripts

L	liquid phase
V	vapour phase
$*$	at bubble formation

References

Abu-Eishah, S. I. 1991 Calculation of vapor–liquid equilibrium data for binary chlorofluorocarbon mixtures using the Peng–Robinson equation of state. *Fluid Phase Equilibria* **62**, 41–52.

Blander, M. & Katz, J. L. 1975 Bubble nucleation in liquids. *AIChE J.* **21**, 833–848.

Carey, V. P. 1992 *Liquid–vapor phase-change phenomena: an introduction to the thermophysics of vaporization and condensation processes in heat transfer equipment.* Washington, DC: Hemisphere.

DeBenedetti, P. G. 1996 *Metastable liquids: concepts and principles.* Princeton University Press.

Elias, E. & Chambré, P. L. 1993 Flashing inception in water during rapid decompression. *Trans. ASME J. Heat Transfer* **115**, 231–238.

Elliot, D. G., Garrison, P. W., Klein, G. A., Moran, K. M. & Zydowicz, M. P. 1984 Flow of nitrogen-pressurized halon 1301 in fire extinguishing systems. Jet Propulsion Laboratory, JPL publication 84-62.

Forest, T. W. & Ward, C. A. 1977 Effect of a dissolved gas on the homogeneous nucleation pressure of a liquid. *J. Chem. Phys.* **66**, 2322–2330.

Forest, T. W. & Ward, C. A. 1978 Homogeneous nucleation of bubbles in solutions at pressures above the vapor pressure of the pure liquid. *J. Chem. Phys.* **69**, 2221–2230.

Grosshandler, W. L., Gann, R. G. & Pitts, W. M. (eds) 1994 Evaluation of alternative in-flight fire suppressants for full-scale testing in simulated aircraft engine nacelles and dry bays. NIST SP 861, US Department of Commerce, Washington, DC.

Gühler, M., Hannemann, R. J. & Sallet, D. W. 1979 Unsteady two-phase blowdown of a flashing liquid from a finite reservoir. In *Two-phase momentum, heat and mass transfer in chemical, process, and energy engineering systems* (ed. F. Durst, G. V. Tsiklauri & N. H. Afgan), vol. 2, pp. 781–795. Washington, DC: Hemisphere.

Holden, B. S. & Katz, J. L. 1978 The homogeneous nucleation of bubbles in superheated binary liquid mixtures. *AIChE J.* **24**, 260–267.

Lienhard, J. H., Alamgir, Md. & Trela, M. 1978 Early response of hot water to sudden release from high pressure. *Trans. ASME J. Heat Transfer* **100**, 473–479.

Modell, M. & Reid, R. C. 1974 *Thermodynamics and its applications.* Englewood Cliffs, NJ: Prentice-Hall.

Modell, M. & Reid, R. C. 1983 *Thermodynamics and its applications*, 2nd edn. Englewood Cliffs, NJ: Prentice-Hall.

Peng, D.-Y. & Robinson, D. B. 1976 A new two-constant equation of state. *Ind. Engng Chem. Fundam.* **15**, 59–64.

Prausnitz, J. M., Anderson, T. F., Grens, E. A., Eckert, C. A., Hsieh, R. & O'Connell, J. P. 1980 *Computer calculations for multicomponent vapor–liquid and liquid–liquid equilibria.* Englewood Cliffs, NJ: Prentice-Hall.

Prausnitz, J. M., Lichtenthaler, R. N. & Gomes de Azevedo, E. 1986 *Molecular thermodynamics of fluid-phase equilibria.* Englewood Cliffs, NJ: Prentice-Hall.

Reid, R. C. 1976 Superheated liquids. *Am. Scientist* **64**, 146–156.

Reid, R. C., Prausnitz, J. M. & Poling, B. E. 1987 *The properties of gases and liquids*, 4th edn. New York: McGraw-Hill.

Skripov, V. P. 1974 *Metastable liquids*. New York: Wiley.

Walas, S. M. 1985 *Phase equilibrium in chemical engineering*. Boston, MA: Butterworth.

Ward, C. A., Balakrishnan, A. & Hooper, F. C. 1970 On the thermodynamics of nucleation in weak gas–liquid solutions. *Trans. ASME J. Basic Engng* **92**, 695–704.

Yang, J. C., Cleary, T. G., Vázquez, I., Boyer, C. I., King, M. D., Breuel, B. D., Womeldorf, C. A., Grosshandler, W. L., Huber, M. L., Weber, L. & Gmurczyk, G. 1995 Optimization of system discharge. In *Fire suppression system performance of alternative agents in aircraft engine and dry bay laboratory simulations* (ed. R. G. Gann), vol. 1, pp. 407–782. NIST SP 890, US Department of Commerce, Washington, DC.

Yang, J. C., Pitts, W. M., Breuel, B. D., Grosshandler, W. L. & Cleveland, W. G. 1996 Rapid discharge of a fire suppressing agent. *Int. Comm. Heat Mass Transfer* **23**, 835–844.

Yang, J. C., Huber, M. L., Vázquez, I., Boyer, C. I. & Weber, L. 1997 Measured and predicted thermodynamic properties of halon alternative/nitrogen mixtures. *Int. J. Refrigeration* **20**, 96–105.